ICRRD Journal
INTERNATIONAL CENTER FOR RESEARCH AND RESOURCES DEVELOPMENT article
ISSN Number: 2773-5958, https://doi.org/10.53272/icrrd, www.icrrd.com

A New and Effective Image Descriptor for Mammography Mass Categorization is RMID

Md Altab Uddin Molla[1*], Souradeep Sarkar[2]

[1 2] *Department of Computational Science, Brainware University, Kolkata, India*

**Corresponding author; Email: altabuddin123@gmail.com*

Received: 02 May 2023 **Accepted:** 28 November 2023
Revision: 30 October 2023 **Published:** 07 December 2023. **Volume**-4, **Issue**-4

Cite as: Molla MAU; Sarkar S. (2023). A New and Effective Image Descriptor for Mammography Mass Categorization is RMID. *ICRRD Journal, 4*(4), 191-201.

ABSTRACT*:* We discuss our most current developments in computer-aided mammography analysis**.** Standard, all-purpose algorithms are commonly used for mammographic picture analysis. We highlight the drawbacks of this strategy and demonstrate how a different, physics-model-based strategy can be created to calibrate the mammographic imaging procedure. This enables us to objectively assess the breast tissue at each and every pixel. For the current experimental framework, we discovered that the proposed RMID outperform spreviously published studies employing convolution neural networks and the manually created histogram techniques Histogram of Gradient Divergence (HGD) and Histogram of Oriented Gradient (HOG), according to the area under the ROC curve. (AUC) (CNN). Additionally, we discovered that utilising only the cardio caudal (CC) view yielded the best AUC value (0.986), as opposed to employing just the medio lateral oblique (MLO) view (0.738), or combining the two views (0.838). The advantage of CC vision over MLO in terms of improved mammography [49] mass categorization is thus demonstrated by these results.

Keywords: *Mammogram image, categorization, picture descriptor, breast cancer*

Introduction

More than 1.5 million women are affected by breast cancer each year, and it is also the main reason why women die from cancer. Breast cancer claimed the lives of 570,000 women in 2015, accounting for 15% of all female cancer deaths. [1]. The most common types of breast cancer, treatable types of cancer if it is found early. Mammography, a cheap X-Ray-based technique, is the main imaging modality for detecting breast tumor. Depending on the ways of processing, mammography can be split into two types: Full Field Digital Mammography (FFDM) and Screen Film Mammography (SFM). Photos are directly kept in the computer's digital storage with FFDM as opposed to SFM, which captures images on film. According to studies that have been described in the literature [2,3], both types of mammography are nearly equally capable of identifying breast lesions that are worrisome. The current study focuses on the SFM pictures that may be found in the BCDR-F03 dataset [27, 29], an example of newest benchmark datasets for breast imaging using film mammography.

These methods are referred to be using computers Diagnosis methods, or, in short, CAD [4], and they have been widely recommended in recent years for computer helped diagnostic of breast cancer. The frequency of false-negative instances is typically reduced through a double-checking procedure by radiologists, but this comes at a clear expense because our health centres generally lack an adequate number of radiologists. As an alternative, a CAD system enables a single radiologist to compare their findings with those of the automated system without the need for a second radiologist to be present. Because of this, there is a necessity for the development of CAD systems.
There are suggested different CAD systems. recently, according to the literature. Three components make up the basic structure of a typical CAD system: (i) processing beforehand mammography pictures to extract ROI (ii) extracting features, and (iii) classification. Recent reports in the literature also mention deep learning-based algorithms. These methods combine steps (ii) and (iii) into a solo stage, replacing the removal of hand-crafted topographies. For improved classification accuracy, image descriptors and clinical data have been incorporated in published publications [4]. The current study focuses on the categorization of masses from mammography images using image descriptors. No clinical data have been taken into consideration.

The Zernike moment-based descriptor was one of the image descriptors described by Constantinidis et al [5] and Belka-Sim et al [6] for classifying masses; other authors [8–12] the persistence of texture categorization of tumor cells and calcification using Haralick characteristics [7]. Other applications of medical imaging have also used Haralick texture features [13], The comparison of texture properties using a deep learning technique comes next. [14]. Different writers also utilise feature descriptors based on wavelet [15,16] and curvelet [17] analysis, and Ramos et al. [18] investigated intensity and texture description combined. Moura and Guevara without using any clinical data, they showed that a deep learning-based method is better to the more conventional hand-examining method by using a complication neural network to distinguish between malignant and benevolent tumors. Convolution neural networks were employed by Arevalo et al. [29]. to distinguish between benign and malignant cancer cells without needing any clinical data.
In this article, we provide a brand-new image descriptor built on multi-resolution radon transform images. Figure 1 displays the proposed method's block diagram. the first dataset of film mammograms is taken into account, and images are classified according to CC and MLO opinions; ROI are subsequently removed, their distinction is improved, and a feature vector is then computed.; finally, classification is performed, and the performance of various classifiers is compared.

For routine screening mammography, the bilateral craniocaudally (CC) and Medio lateral oblique (MLO) views are regarded as standard views. All clients who undergo routine screening typically use the views. These 4 images are included in screening mammography, barring any contraindications.
The long-term sections of the essay are arranged as monitors: Sec. 2 discusses the proposed RMID and the construction of classifiers; Sec.3 reports descriptions of the datasets and experimental information, comparative analysis of the experimental design and findings. Last, Sec. 4 brings the essay to a close.

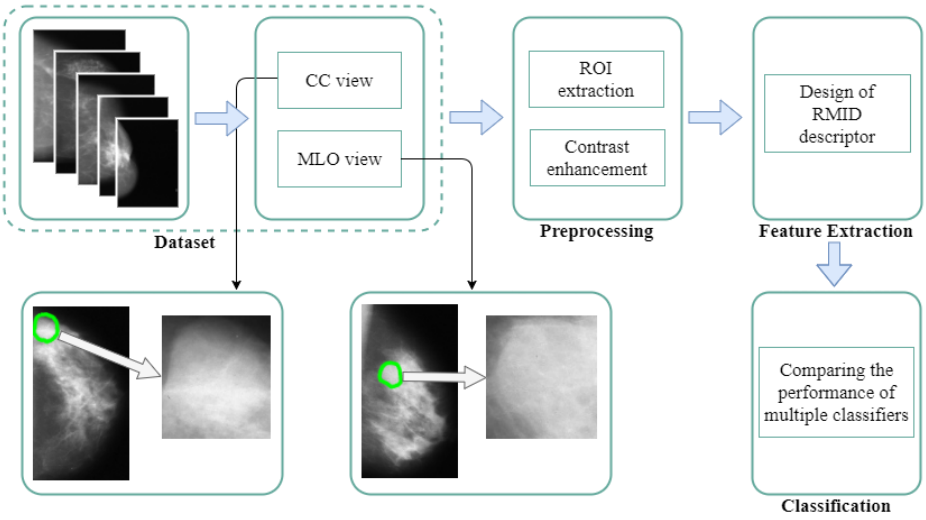

Block schematic of the suggested technique, Figure 1.

Summary of contributions

As previously indicated, we suggest RMID as a new feature definition for classifying mammography masses. Our goal is to specifically use this innovative image descriptor to categorise malignant and benign masses from mammography pictures. In the subsection that follows, we go into great detail on RMID.

RMIDN's guiding principles and architecture

Transform for radon and multiple resolution analysis are both used in RMIDN. Below is a description of these strategies' fundamental principles.

Radon conversion. As shown in Figure 2, where part (a) depicts the primary and component projections (b) depicts the various angles taken into consideration for the current task, the Radon flip is an integral part of effective. It consists of several projections of a design formed at altered positions. [19]. A task f (x, y) is transferred to a different utility R (x, y), It is displayed in the plane's 2D arc space, For the specified set of angles, its value along a line corresponds to the line fundamental of the corresponding utility along that line. Otherwise, it is possible to consider an example of a pattern's radon transform f (x, y) as the projection of all points that are not zero for a specific set of angles. The result of the projector is the amount of the non-zero facts for each direction of the outline of pictures. (viewpoint from 0 to 180). Matrix is ultimately created. The f (x, y) integral over a path is related to the matrix elements.

$Lin(\rho, \vartheta)$ marked as $\rho = x\cos\vartheta + y\sin\vartheta$ and let it may be as

$$fR(\rho, \vartheta) = \int_{-\infty}^{\infty}\int_{-\infty}^{\infty} f(x, y)\delta(x\cos\vartheta + y\sin\vartheta - \rho)dxdy$$

Let $\delta(.)$Dirac delta function, $\delta(x) = 1$, if $x = 0$. Also,$\vartheta \in [0, \pi]$ and $\rho \in]-\infty, \infty[$. Lini I should be in a form for the radon transform (ρ_i, ϑ_i).

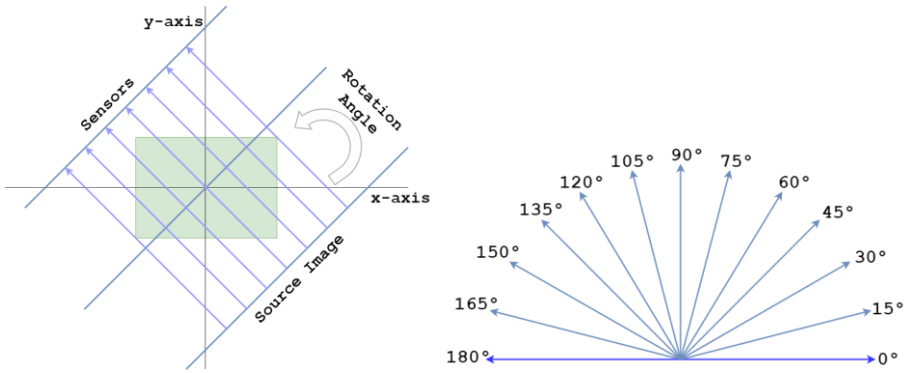

(b)

Fig. 2: Radon transform theory illustration The current work's computation of the line integral took into account (a) the generation of the radon spectrum and (b) a variety of angular direction

multi-resolution evaluation. The wavelet convert is used to denote the time-frequency response of a signal, in this case a picture. In the current work, discrete wavelet techniques known as Daubechies wavelets [20] are employed. When performing multi-resolution analysis, wavelets have the benefit of being computationally simple and requiring little in the way of time or resources. The most vanishing moments possible for a given support define these orthogonal wavelets. For further analysis, we divide an image into several frequencies and resolutions. The Daubechies wavelet family is referred to as "dbN," where "db" refers to the wavelet family and "N" refers to the quantity of vanishing moments. Combining various components with various coefficients can represent an image. The coefficients of a component of a picture have been determined to be constant, linear, and quadratic. captured by db1, db2, and db3 in the current work's wavelet decomposition at level 1. This procedure generates four sub-band images for each of the db2, db3 and db1 parts, For a max of 12 sub-band pictures, these are the approximation factors (cA), vertical factors (cV), diagonal factors (cD)and horizontal factors (cH).

RMID's structure. To construct RMID, the radon transform idea is merged with multi-resolution analysis. Both benign and malignant tumors have various textural patterns. In contrast to benevolent masses, whose limit areas are more symmetrical in form, the malignant mass region is more irregular. Several pixels' line integral over a given direction is calculated using the Radon transform**.** Therefore, if the radon transform is calculated with regard to both benign and malignant tumors, Each time, The line integral will have a different value. The radon spectra of benign and malignant tumors is depicted in Fig. 3: Fig. 3(a) depicts a benign tumors, and Figure 3(c) displays its radon spectrum. Figure 3(b) depicts a malignant tumor, and Figure 3(c) displays its radon spectrum 3(d).
For picture decomposition, a number of techniques are available, including quad-tree decomposition with n-fold division. Here, we selected wavelet because wavelet decomposition allows for many directional approximations. We compute the radon spectrum derived from each semi picture, i.e. on cH, cV, cD and cA. Radiation spectrum of radon used to create the feature vector are then used to calculate statistical values.

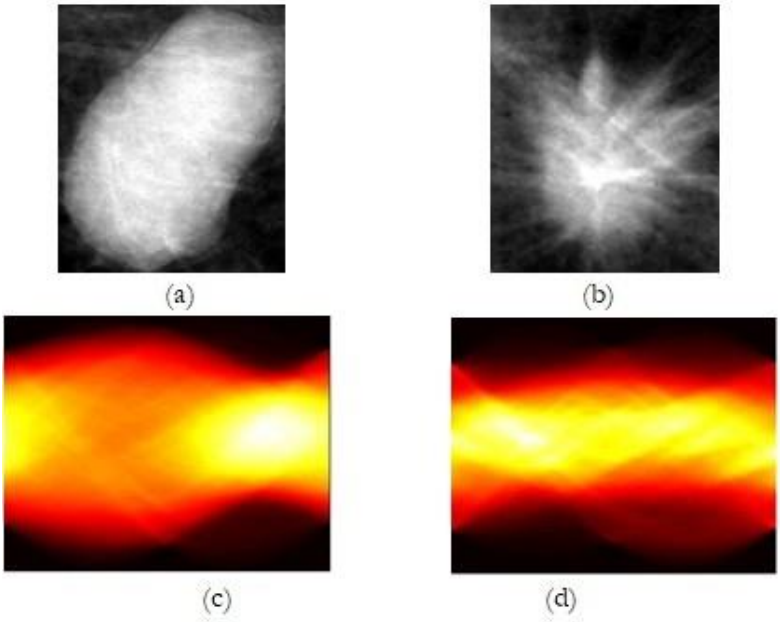

Figure 3. Display of the radon spectrum and the ROI taken from mammography images. (a) compassionate tumors, (b) malignant tumors, (c) Radiation range of figure a, (a) Radiation range of figureb

Generating feature vectors : The summary of the RMID-based feature vector creation process:

First, ROIs from the original mammography images were recovered, and then each ROI underwent contrast enhancement. Then, a grayscale image of the improved ROI was saved.
Wavelet decomposition for db1, db2, and db3 for level 1 was performed using the Daubechies technique. For each coefficient, this phase yields four subband images, giving rise to a overall 12 subband pictures.
The Radon transform is used. to the 12 sub-band pictures created in the previous stage as well as the original ROI image. We produce a total of 13 radon spectra at this stage.
We compute one energy and three statistical feature values for each of the 13 radon spectrum. This process creates 52 characteristics in total (04 13). Then, using the original grayscale image as input, comprising entropy, mean, standard deviation, and maximum radon spectrum coefficient, we construct statistical characteristics, yielding a feature vector with a total dimension of 56 (52 + 04).

Classifiers
Six distinct classifiers were trained and employed in our investigation to categorise the masses. They are the Multilayer Perceptron (MLP), Support Vector Machine (SVM),Linear Discriminant Analysis (LDA), the Random Forest(RF) and the Bayesian Network (BN). To determine which classifier performs the best, we compare their performances. Following is a brief explanation of these classifiers.

Bayesian network. We employed K2, a well-known an efficient technique based on scores that creates a directed acyclic graph to represent the underlying distribution, for the Bayesian network (BN). Details are available in [23].

Linear discriminant analysis, using a shared covariance matrix and numerous mean vectors for different classes. we describe the data in linear discriminant analysis [24] as a collection of normal multivariate distributions. The hyper-plane (HP) used by LDA to divide the feature space has two sides that correspond to two classes. Depending on the plane's side, the classes are located, the test dataset is used to identify the class pattern.

Logistic. Logistic regression classifies observations into distinct groups using a set of classifications [43]. A logistic function (sigmoid) is used by the logistic classifier to alter its output before returning a hazard value. Then, at least two classes are transformed into this probability value [25].

Support vector machine. Through the creation of a hyper-plane (HP) taking place on the heavy feature galaxy, SVM classifies the data. You can use a variety of linear and nonlinear kernels. We employed SVM customized by a linear kernel for the current work because it is quick and produced good outputs.

Multiple-layer perceptron's Among the most employed classifiers is MLP. In this instance, a configuration of 56-hl-2 was used, wherever 56 represents the amount attribute values, the amount(hl) of secret layer nodes, as well as 2 is the number of classes. By considering the interactions between the output classes and the feature dimension (56), hl can be computed empirically (two). The value of hl in our experiment is assumed to be 29, or (56+2)/2.

irregular forest theoretically, a group of result trees that have not been pruned and were trained selecting random features from bootstrap samples, each tree selects a favorite class, and the decision is made by summing all the votes. [26].

Investigation and experimentation

Setup of the dataset

In our study, we used the BCDR-F03 [28,29] benchmark dataset for film mammography from the Digital Repository for Breast Cancer[58], a thorough public database of breast cancer patient records from Portugal [4]. One of the most recent benchmarked datasets for film mammography, the BCDR-F03, has 668 film mammogram pictures. 736 biopsy-confirmed tumors, from 344 patients, of which 426 were benign and 310 were cancerous., were found among the 668 images. Consequently, a single image frequently incorporates many masses.

For the sake of this work, we assumed that each image contained one mass, for a total of 668 masses. After a few photos with extremely low resolution were removed from the 668 masses, 662 photographs were left. The samples are given in two views: the mediolateral oblique (MLO) view and the carniocaudal (CC) view. In our statistics, there are 328 CC views and 334 MLO views. The lesions are indicated on the various mammography pictures in Figure 4.

Two steps during the preparation procedure are (i) ROI abstraction and (ii) gap amplification. The radiologist's information was used to extract the ROI, and The ROI coordinate data are given with the BCDR-F03 dataset in an annotated file. ROIs were retrieved and stored using automated methods in various files based on the various view kinds. Additionally, They were separated into benign and malignant class files. Due to a number of factors, the original film mammograms have relatively poor contrast. (poor lighting, orientation, etc.), ROIs contrast enhancement was next carried out.

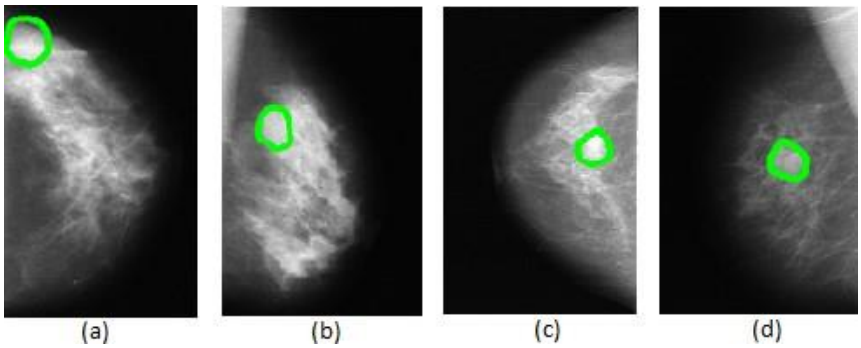

Fig. 4. various mammography pictures (a) L C C, (b) L O, (c) R C C, (d) R O. The ROI is shown by the green border.

By removing the average of the image's intensities from each pixel, contrast is improved One initial ROI and its improved contrast variant are shown in Figure 5

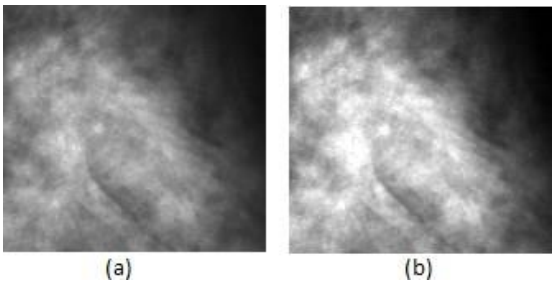

Fig. 5 Enhancing the contrast, (a) Real ROI with low gap, (b) distinction enhancing picture

Metrics for evaluation

We utilize the Area Under the Curve (AUC) of the Worker Distinguishing to assess how well the system works. The ratio of true positives to false positives is plotted to create the ROC curve. An prior study on this dataset also used the AUC as a measure of discrimination [4, 29], allowing a comparison with our method.

Table 1. output of mammogram mass categorization for the test dataset using the MLO, CC, and combined (MLO+ CC) perspectives, as slow in AUC

Classifier	C C	M L O	MLO+C C
(BN)	0.934	0.690	0.816
(LDA)	**0.986**	0.672	0.807
Logistic	0.958	0.674	0.811
(SVM)	0.977	0.682	0.783
(MLP)	0.985	0.618	0.813
(RF)	**0.986**	**0.738**	**0.838**

Evaluation plan and setup of the system

Three distinct kinds of tests were conducted: I mammography mass classification using both views concurrently, tumors classification as the CC view, mass classification after the MLO view, and mass classification from the mammography. For fair comparison, the dataset in each example was split into a 60:40 ratio (utilizing 40% of the data for testing and 60% for training) [4, 27, 29]. Regarding the tools, MATLAB 2017b software was used throughout all experiments on a system.

Findings and interpretation

Within this research, we offer a brand-new picture descriptor for categorizing mammography masses., but we also examine how well various classifiers perform. Additionally, an examination of the ideal image view for mass classification is carried out. 3 altered mammography opinions[45]—CC, MLO, and both joined—are examined, and the outcomes of 6 diverse classifiers—BN, Logistic, LDA ,SVM, MLP, and RF in Table 1 for each classifier (The greatest values are shown in bold). LDA and RF perform the best among the six classifiers, with an AUC of 0.986, according to the table's first column, which displays the output of the CC view. When both views are taken into account (both CC and MLO images are taken into consideration), RF also has the greatest AUC of 0.838 for the MLO view. Based on these findings, it is feasible to say that RF performs regardless of visual view, the best.

Previous relevant work – analogy.

i) Results of three separate mammography pictures using 6 verity classifiers (BN, Logistic, MLP, LDA, SVM and RF) (MLO, CC and both joined). LDA and RF outperform the other six classifiers, as shown in the first column of the table's findings on behalf of the CC opinion. RF also has the greatest AUC of 0.838 for the MLO view when both views (both CC and MLO photos are taken into account) are included. These results allow us to conclude that RF performs best independent of image view.

ii) The subset of the BCDR-F03 dataset known as the BCDR-F01 dataset, was used to test a histogram-based image descriptor called HGD suggested by Moura et al. [4] prior to the completion of this work. The maximum AUC was recorded as 0.787 by HDG and 0.770 by conventional HOG. However, clinical data was also included, thus these findings are not entirely dependent on image description. Arevalo et al. recently suggested a deep learning-based method using the BCDR-F03 dataset. They reached an AUC of 0.821 by utilizing a convolution neural network (CNN), and then combine

Hand-crafted methods [29]	HDG	0.826
Deep-learning based method [27] [29]	CNN	0.821
RMID[]	RMID	**0.838**
Proposed Techniques	RMIDN	**0.844**

Table 2. Performance evaluation of the suggested method against benchmark outcomes (CC+MLO viewpoints merged)

Approaches	A U C

The general AUC was raised to 0.826, demonstrating progress of 0.40% thanks to the hand-crafted HGD features. However, these two efforts are not truly comparable because they used

different experimental frameworks; for example, [4] examined an 80:20 data split for training whereas [27, 29] evaluated a 60:40 split.
Table 2 displays the stated outcomes and enables a qualitative evaluation of our approach (established on the current new framework and considerations). When compared to the conventional techniques, the suggested RMIDN performs noticeably better, demonstrating its efficacy as an image identifier for mass classification.

Conclusions and next steps

Automatic diagnosis of breast cancer from mammography pictures will undoubtedly assist radiologists by verifying their findings. There are several approaches suggested in the literature for classifying mammography masses from film mammogram pictures, However, these descriptors typically work effectively when combined with clinical data. In this work, we recommend an unique picture descriptor that functions effectively in the absence of clinical data. The combined AUC for the proposed RMIDN and the proposed random forest classifier is 0.843 for the combined view, 0.738 for the MLO opinion, and 0.986 for the CC vision. The CC view is more useful for classifying mammography mass than the MLO one. In this research, we discovered that CC opinion outperforms MLO by 33.60%.
In order to back up the decisions drawn in this study, namely that the RMID descriptor is superior and the CC and MLO perspectives are uniquely capable of discrimination, — We want to carry out a statistical analysis of the results after testing the suggested descriptor's effectiveness on other openly accessible film mammography datasets. Additionally, we want to evaluate RMID performance in conjunction with clinical data and contrast the effectiveness of digital and film mammography.

Declarations

The manuscript has not been submitted in any other journal or conference.

Conflicts of Interest

There are no conflicts to declare.

Funding: The study received no funding from any source.

Acknowledgment: The authors extend their sincere appreciation to the editor and the anonymous reviewers for providing valuable feedback that significantly contributed to the improvement of this paper.

References

Skaane, P., Hofvind, S., Skjennald, A.: Randomized trial of screen-film versus full-field digital mammography with soft-copy reading in population-based screening program: follow-up and final results of Oslo II study. Radiology. vol. 244(3), pp.708-17, 2007.

Pisano, E.D., Hendrick, R.E., Yaffe, M.J., for the Digital Mammographic ImagingScreening Trial (DMIST) Investigators Group: Diagnostic accuracy of digital ver-sus film mammography: exploratory analysis of selected population subgroups in DMIST. Radiology. vol. 246(2), pp.376-83, 2008.

Moura, D. C., Lopez, M. A. G.: An evaluation of image descriptors combined withclinical

data for breast cancer diagnosis. Int. Journal of Comp. Assisted Radiology and Surgery, vol. 8, pp.561-574, 2013.

Constantinidis, A.S., Fairhurst, M.C., Rahman, A.F.R.: A new multi-expert decisioncombination algorithm and its application to the detection of circumscribed massesin digital mammograms. Pattern Recognition, vol. 34(8), pp.1527–1537, 2001.

Belkasim, S.O., Shridhar, M., Ahmadi, M.: Pattern-recognition with moment in-variants—a comparative-study and new results. Pattern Recognition, vol. 24(12),pp.1117–1138, 1991.

Haralick, R.M., Shanmuga, K., Dinstein, I.: Textural features for image classifica-tion. IEEE Tran. Syst Man Cyb, vol. 3(6), pp.610–621, 1973.

Yu, S. Y., Guan, L.: A CAD system for the automatic detection of clustered micro-calcifications in digitized mammogram films. IEEE Tran. Med. Imaging, vol. 19(2),pp.115–126, 2000.

Dhawan, A.P., Chitre, Y., Kaiser, B. C., Moskowitz, M.: Analysis of mammographicmicrocalcifications using gray-level image structure features. IEEE Trans Med Imag-ing, vol. 15(3), pp.246–259, 1996.

Wang, D., Shi, L., Ann, H. P.: Automatic detection of breast cancers in mammo-grams using structured support vector machines. Neurocomputing, vol. 72(13–15), pp.3296–3302, 2009.

Dua, S., Singh, H., Thompson, H. W.: Associative classification of mammograms using weighted rules. Expert Syst Appl, vol. 36(5), pp.9250–9259, 2009.

Sahiner, B., Chan, H. P., Petrick, N., Helvie, M. A., Hadjiiski, L. M.: Improvementof mammographic mass characterization using spiculation measures and morpho- logical features. Med Phys, vol. 28(7), pp.1455–1465, 2001.

Claudia, M., Enrique, A., Maria T., V´ıctor G. C.: Tissues Classification of the Cardiovascular System Using Texture Descriptors. MIUA 2017: Medical Image Un- derstanding and Analysis, pp.123-132, 2017.

Alison, O. N., Matthew, S., Erin, B., Keith, G.: A Comparison of Texture Features Versus Deep Learning for Image Classification in Interstitial Lung Disease. MIUA 2017: Medical Image Understanding and Analysis, pp. 743-753, 2017.

Ferreira, C. B. R., Borges, D. B. L.: Analysis of mammogram classification using a wavelet transform decomposition. Pattern Recogn. Lett., vol. 24(7), pp.973–982,2003.

Rashed, E.A., Ismail, I.A., Zaki, S.I.: Multiresolution mammogram analysis in multilevel decomposition. Pattern Recogn. Lett., vol. 28(2), pp.286–292, 2007.

Meselhy, E. M., Faye, I., Belhaouari, S. B.: A comparison of wavelet and curvelet for breast cancer diagnosis in digital mammogram. Comput BiolMed, vol. 40(4), pp.384–391, 2010. oi:10.1016/j.compbiomed.2010.02.002

Ramos-Pollan, R., Guevara-López, M., Suárez-Ortega, C., Díaz-Herrero, G.,

Franco-Valiente, J., Rubio-del-Solar, M., de Posada González, N., Vaz, M., Loureiro, J., Ramos, I.: Discovering mammography-based machine learning classifiers forbreast cancer diagnosis. J Med. Syst., vol. 36(4), pp.2259-69, 2011.

Deans, S.R.: Applications of the Radon Transform. Wiley Interscience Publica- tions, New York, 1983.

Mallat, S. G.: A theory for multiresolution signal decomposition: the wavelet representation. IEEE Tran. on Pattern Anal. and Machine Intelligence. vol. 11(7), pp.674–693, 1989.

Huhn, J., Hullermeier, E.: FURIA: an algorithm for unordered fuzzy rule induc- tion," Data Min. Knowl. Discov., vol. 19(3), pp.293-319, 2009.

Bielza, C., Li, G., Larrañaga, P.: Multi-Dimensional Classification with Bayesian Networks, International Journal of Approximate Reasoning, vol. 52, pp.705-727, 2011.

Mika, S., Ratsch, G., Weston, J.: Fisher Discriminant Analysis with Kernels. Conference on Neural Networks for Signal Processing IX: pp.41–48, 1999.